

This discussion paper is/has been under review for the journal Ocean Science (OS).
Please refer to the corresponding final paper in OS if available.

Near-surface diurnal warming simulations: validation with high resolution profile measurements

B. Scanlon¹, G. A. Wick², and B. Ward¹

¹School of Physics and Ryan Institute, National University of Ireland, Galway, University Road, Galway, Ireland

²NOAA ESRL PSD, 325 Broadway Boulder, CO 80305, USA

Received: 28 September 2012 – Accepted: 5 December 2012 – Published: 20 December 2012

Correspondence to: B. Ward (bward@nuigalway.ie)

Published by Copernicus Publications on behalf of the European Geosciences Union.

OSD

9, 3851–3878, 2012

Near-surface diurnal warming simulations

B. Scanlon et al.

Title Page

Abstract

Introduction

Conclusions

References

Tables

Figures

◀

▶

◀

▶

Back

Close

Full Screen / Esc

Printer-friendly Version

Interactive Discussion



Abstract

Sea surface temperature (SST) is an important property for governing the exchange of energy between the ocean and the atmosphere. Common in-situ methods of measuring SST often require a cool-skin and warm-layer adjustment in the presence of diurnal warming effects. A critical requirement for an ocean sub-model is that it can simulate the change in SST over diurnal, seasonal, and annual cycles. In this paper we use high-resolution near-surface profiles of SST to validate simulated near-surface temperature profiles from a modified version of the Kantha and Clayson 1-D mixed layer model. Additional model enhancements such as the incorporation of a parameterisation of turbulence generated by wave breaking and a solar absorption model are also validated. The model simulations show a strong variability in highly stratified conditions, with different models providing the best results depending on the specific criteria and conditions. In general, the models with enhanced wave breaking effects tended to underestimate the temperature profile measurements while the more coarse baseline and blended approaches produced the most accurate comparisons with the in-situ SST data.

1 Introduction

Accurate measurements of sea surface temperature (SST) for the upper ocean are important for air-sea exchange of heat (Fairall et al., 1996b) and gas (Ward et al., 2004a). It has been shown that SST values with an accuracy of $\pm 0.2\text{K}$ are required to compute the air-sea heat fluxes to an accuracy of 10Wm^{-2} (Fairall et al., 1996a). Bulk formula heat flux calculations rely on SST values to compute sensible and latent turbulent heat fluxes as well as emitted longwave radiation from the ocean surface, and these models are most sensitive to SST variability in the lower latitudes. According to Fairall et al. (1996b) the most appropriate value of SST for these formulae is the temperature of the cool-skin layer, known as the skin temperature (SST_{skin}). The cool-skin layer (or

OSD

9, 3851–3878, 2012

Near-surface diurnal warming simulations

B. Scanlon et al.

Title Page

Abstract

Introduction

Conclusions

References

Tables

Figures

◀

▶

◀

▶

Back

Close

Full Screen / Esc

Printer-friendly Version

Interactive Discussion



the molecular sublayer) is ~ 1 mm thick, and is the upper most layer of the sea surface and is in direct contact with the atmosphere. The skin temperature is cooled by the combined effects of the net longwave radiative flux, the sensible heat flux and the latent heat flux and is typically 0.1–0.5 K lower than the temperature of the subskin layer immediately below (Wick et al., 1996; Donlon et al., 2002). The cool skin is almost always present, although its total effect may be compensated by the presence of a warm-layer (Fairall et al., 1996b). Common in situ methods of SST measurement obtain temperature at a depth, often 1–4 m, called SST_{depth}, or commonly the bulk temperature measurement. These bulk temperatures are the most commonly available measurements obtained from buoys and ships (Gentemann et al., 2009). It is often required that these bulk measurements be adjusted for diurnal warm-layer and cool-skin effects.

In the upper ocean, diurnal warming cycles occur due to the solar heating and oceanic heat loss fluctuations (Price et al., 1986) and are responsible for high variations of SST. For example, in summer heating conditions with low wind, the depth of the diurnal warm-layer can typically be on the order of 1 m (mean depth), and the surface amplitude (skin temperature minus bulk temperature) can be as large as 3 K (Stramma et al., 1986; Soloviev and Lukas, 1996). In such conditions, turbulent mixing near the surface is mainly driven by wind-induced shear and convection. This convection is driven by densification due to evaporation and possible net surface cooling. Daytime solar heating effects within a stratified upper ocean are isolated to the surface layers. The heating of these layers create a positive buoyancy flux which restricts deepening of the warm-layer (Soloviev and Lukas, 1996), further enhancing the effects of stratification. In moderate wind conditions, solar heat is mixed vertically to a greater depth than what can be achieved directly by radiation. In such cases, the positive surface buoyancy fluxes are overcome by wind driven shear which deepens the diurnal warm-layer typically to 10 m depth. In turn, the surface amplitude is typically reduced to 0.2 K (Price et al., 1986).

Near-surface diurnal warming simulations

B. Scanlon et al.

[Title Page](#)[Abstract](#)[Introduction](#)[Conclusions](#)[References](#)[Tables](#)[Figures](#)[◀](#)[▶](#)[◀](#)[▶](#)[Back](#)[Close](#)[Full Screen / Esc](#)[Printer-friendly Version](#)[Interactive Discussion](#)

Near-surface diurnal warming simulations

B. Scanlon et al.

[Title Page](#)[Abstract](#)[Introduction](#)[Conclusions](#)[References](#)[Tables](#)[Figures](#)[◀](#)[▶](#)[◀](#)[▶](#)[Back](#)[Close](#)[Full Screen / Esc](#)[Printer-friendly Version](#)[Interactive Discussion](#)

Previous studies using models and near-surface temperature profile measurements have demonstrated the potential for significant variability in the near-surface temperature especially during the daytime at low winds and with strong solar heating (Fairall et al., 1996a; Soloviev and Schluessel, 1996; Webster et al., 1996; Donlon, 1999; Gentemann and Minnett, 2009; Gentemann et al., 2009). The goal of this paper is to compare model simulations to observed high resolution temperature profile measurements in low to moderate wind and high solar irradiance environments, in order to evaluate the model skill to accurately reproduce the measured temperature profile.

Observed temperature profiles of the upper 5 m of the ocean were measured by the Skin Depth Experimental Profiler (SkinDeEP) (Ward et al., 2004b) and also by its successor the Air-Sea Interaction Profiler (ASIP) (Ward et al., 2012). The profiles presented here were obtained during three separate field experiments: Gulf of California in 1999 (hereafter GC99), Gulf of Lions (Mediterranean) in 2003 (hereafter GL03), and the Indian Ocean in 2007 (hereafter IO07). SkinDeEP is an autonomous profiler capable of measuring temperature to a sub-centimetre resolution. With a typical rise velocity of 0.5 ms^{-1} , the resolution is 3 mm (see Ward et al. (2004b) for a complete description of SkinDeEP). ASIP is similar in concept to SkinDeEP, but has a much larger sensor range, can profile to 100 m, and has a larger battery capacity. Coupling the high resolution profile data from the near-surface along with M-AERI radiometric data of the true skin temperature, provides a complete temperature profile of the upper ocean.

This article attempts to validate the model simulations of a 1-dimensional second moment turbulence closure mixed layer model based on Kantha and Clayson (1994) for the GC99, GL03, and IO07 time periods, using available meteorological data and bulk measurements. Further refinements to the model including wave breaking effects (Kantha and Clayson, 2004) and improved solar transmission (Ohlmann and Siegel, 2000). Section 2 discusses the cruise data and instrumentation. Section 3 provides a theoretical background for the models used in this study. Section 4 shows the results from the comparisons of the measured SkinDeEP data and the modelled simulations, followed by our conclusions.

2 In-situ data

The GC99 dataset was obtained over a 12 day period in October 1999 near Baja California. Ten successful deployments of SkinDeEP were obtained, leading to a total of 976 high resolution upper ocean profiles. The deployments were carried out from the R/V *Melville* mainly during early afternoon periods when diurnally-induced stratification was high. Over the twelve days, the solar heat flux was high and the wind varied from 1 to 9 ms⁻¹. For each day the downwelling shortwave radiation reached over 800 W m⁻² and wind speeds were relatively low with a mean range of 3.5 ± 1.8 ms⁻¹ across all the deployments. Deployment 10 occurs in idealised weather conditions for this study with a mean wind speed of 1.1 ms⁻¹ and a mean shortwave radiation of 802 W m⁻² (peaking at 912 W m⁻²) (Fig. 1). A full description of the GL99 meteorological conditions can be obtained in Ward (2006).

Additional data is provided by SkinDeEP from the GL03 experiment in the Gulf of Lions onboard the R/V *Urania* during April 2003. The profiler obtained 576 different profiles during three deployments over three days. Due to a technical issue during the first two deployments, SkinDeEP did not record data in the upper metre. The error was corrected before the final deployment took place and we limit our analysis to this dataset here. This deployment represents the situation where a well mixed night-time water column is being subjected to strong morning-time solar heating. Solar shortwave radiation rises from a minimum value to 876 W m⁻². The mean wind speed is 6.29 ± 0.52 ms⁻¹ for the period (Fig. 1).

The data collected from the IO07 cruise represents a high resolution view of the temperature structure in a highly stratified area of the Indian-Pacific warm pool, the “Seychelles-Chagos Thermocline Ridge” (Vialard et al., 2009). The deployment described here occurred on the 8/9 February and resulted in 72 profiles captured in stratified conditions. The period started at 19:02 and finished at 07:21 the next morning. The mean wind speed was 4.35 ± 0.38 ms⁻¹. The start of the deployment was during nighttime, and measurements ceased when the the downwelling irradiance reached

OSD

9, 3851–3878, 2012

Near-surface diurnal warming simulations

B. Scanlon et al.

Title Page

Abstract

Introduction

Conclusions

References

Tables

Figures

◀

▶

◀

▶

Back

Close

Full Screen / Esc

Printer-friendly Version

Interactive Discussion



102 W m⁻² (Fig. 1). Table 1 displays additional information regarding the GC99, GL03 and IO07 deployments.

2.1 SST measurements

The surface temperature profiles were obtained from either SkinDeEP (Ward et al., 2004b) or ASIP (Ward et al., 2012). Both of these instruments are autonomous vertical profilers designed to study the upper ocean with high resolution sensors. For this study, we are concerned with temperature profiles in the upper 5 m, which are provided by the FP07 thermometer mounted on both profilers.

SkinDeEP has the ability to obtain more than 100 consecutive profiles without intervention and contains a CPU capable of high-frequency sampling and data storage (Ward, 2006). Autonomous profiling is accomplished with a buoyancy system composed of an inflatable neoprene sleeve attached to the shell of the profiler, 2 solenoids and an air pump. The sleeve can be inflated using the air pump thus changing the volume of the profiler while keeping its mass constant, which alters its buoyancy. SkinDeEP maintains an upright position in operation due to its low centre of gravity, achieved by locating the batteries towards the bottom of the instrument. While in operation, it was attached to a spar buoy via 50 m of a synthetic, high breaking strain tether line. Profiling started with the instrument sinking to its programmed depth which was monitored by the onboard external pressure sensor, at which point the bladder inflated and temperature measurements were acquired as it rose to the surface. The temperature data was provided with the FP07 thermistor, which was calibrated against a slower, accurate thermometer.

ASIP is an autonomous vertically profiling instrument designed to profile from below so as to provide undisturbed measurements all the way to the surface. It is equipped with high resolution sensors for the measurement of temperature, salinity, light, oxygen, and turbulence. There are three thrusters which submerge it to a programmed depth (maximum 100 m), whereupon it ascends through the water column towards the

Near-surface diurnal warming simulations

B. Scanlon et al.

Title Page

Abstract

Introduction

Conclusions

References

Tables

Figures

◀

▶

◀

▶

Back

Close

Full Screen / Esc

Printer-friendly Version

Interactive Discussion



surface under its own buoyancy, recording data at 1000 Hz, generating 192 kbytes per second which is stored with on a single board computer.

The skin temperature for both cruises was continuously measured by the Marine-Atmospheric Emitted Radiance Interferometer (M-AERI, Minnett et al., 2001); a passive infrared radiometric interferometer which makes radiance measurements in the 500 to 3000 cm^{-1} wave number range with a resolution of 0.5 cm^{-1} . The radiometer comprises of a gold rotating mirror that allows for both sea and sky views at complementary angles to nadir and zenith. The accuracy of the derived SST measurements are better than 0.05 K (Minnett et al., 2001). Real time calibration is continuously carried out by viewing two internal blackbody cavities, one set to 60°C and the other to ambient temperature.

The M-AERI skin temperature and SkinDeEP/ASIP temperature profile measurements used collectively create a high resolution temperature profile of the upper few metres of the sea surface.

3 Model

Five variations of the Kantha and Clayson (1994) (KC94 hereafter) second moment closure, one dimensional mixed layer model provide one-minute resolution simulations of the upper ocean for the durations of the GC99, GL03 and IO07 cruises. The first, or “baseline” configuration most closely corresponds to that described in KC94. The model name is shortened to “Base” for representation in tables and plots. The basic turbulence scheme is that of KC94, but the vertical resolution is enhanced to simulate the details of the near-surface temperature profile. A nine-wavelength band solar absorption model of Paulson and Simpson (1981) (PS81 hereafter) is used in this configuration to account for solar heating effects within the water column. It is a common assumption in ocean modelling to assume that the Karman–Prandtl law of the wall is valid near the air-sea interface. This assumption works well in shear flows adjacent to a rigid boundary but fails in the presence of breaking waves near the surface (Craig and Banner, 1994). This is due to the turbulent kinetic energy (TKE) equation being

Near-surface diurnal warming simulations

B. Scanlon et al.

Title Page

Abstract

Introduction

Conclusions

References

Tables

Figures

◀

▶

◀

▶

Back

Close

Full Screen / Esc

Printer-friendly Version

Interactive Discussion



Near-surface diurnal warming simulations

B. Scanlon et al.

Title Page

Abstract

Introduction

Conclusions

References

Tables

Figures

◀

▶

◀

▶

Back

Close

Full Screen / Esc

Printer-friendly Version

Interactive Discussion



based on local shear production and dissipation near the surface. Kantha and Clayson (2004) (hereafter KC04) suggests that the influence of wave breaking strongly elevates the dissipation rate in the upper few metres of the ocean and the effects cannot be ignored (see also Terray et al., 1996; ?). A second version of the model incorporating the TKE equation of KC04 to account for these effects is termed the “enhanced wave breaking model” (shortened to EWB in figures). This addition incorporates TKE injection parameters due to breaking waves and langmuir circulation. Weller and Price (1988) found that stratified thermal layers in shallow diurnal mixed layers can be rapidly destroyed by langmuir circulation. Thus the inclusion of a parameter for langmuir cells is important. The new parameterization for TKE input at the surface is proportional to a power law of the water-side friction velocity u_* . The inclusion of these parameters increases TKE and dissipation rates in the upper ocean, leading to enhanced mixing in the mixed layer. KC04 reported the effects of including langmuir circulation in the model resulted in lower SST values. The reader is referred to Kantha and Clayson (2004) for more information.

The third model used in this study is named the “blended model” (shortened to “blend” in figures). This model transitions between the use of the baseline model and the enhanced wave breaking model at a wind speed of 2 m s^{-1} . The turbulence scheme below 2 m s^{-1} is that of the baseline model while it shifts toward that of the enhanced wave breaking model at higher winds. This blending was introduced in an attempt to reproduce the range of diurnal warming amplitudes observed in previous shipborne observations of the surface temperature (not shown). The turbulence coefficients are also revised within this model to follow Kantha (2003).

Solar insolation is a very important parameter for the effects of diurnal warming. It has been reported that between 60 %–90 % of solar irradiance is attenuated within the upper 10 m of the ocean (Ohlmann et al., 1998). Variations in the assumed absorption rate of insolation can have a significant effect on the simulated profiles. The “PS81” 9-band solar transmission model, of Paulson and Simpson (1981) is used for the three models described so far. This solar transmission model computes solar transmission

through the air–sea interface by fixing the sea surface albedo to a constant value of 0.055 which has been stated to produce instantaneous errors of $\pm 40 \text{ W m}^{-2}$ (Ohlmann and Siegel, 2000). The reader is referred to Fairall et al. (1996b) and Ohlmann and Siegel (2000) for further information.

5 The fourth model version tested incorporates a more recent solar absorption profile developed by Ohlmann and Siegel (2000) (hereafter OS00) along with the “enhanced wave breaking model” and is called the “enhanced solar transmission model” (shortened to “EST” in figures). It is a two-equation solar transmission parameterization that depends on upper ocean chlorophyll concentration, cloud amount and solar
10 zenith angle. In a high solar insolation and low wind condition study carried out by OS00, they found the new parameterization to give a mean 12 W m^{-2} reduction in the quantity of solar radiation attenuated in the top few metres of the ocean compared with previous parameterizations. The new transmission parameterization gives a slightly deeper warm-layer and a decrease in the warm-layer temperature correction which
15 often reaches 0.2 K (Ohlmann and Siegel, 2000).

The final version of model tested is an enhancement of the “blended model”. It transitions between the baseline and enhanced wave breaking models in the same fashion as the blended model but also incorporates the OS00 two-equation solar transmission model described for the enhanced solar transmission model in place of the PS81 9-
20 band model. It is called the “blended solar transmission model” (shortened to BST in figures). A summary of the main differences between the 5 model versions discussed is shown in Table 2.

25 The air-sea heat fluxes used to force the Kantha and Clayson model versions were calculated using the TOGA COARE Bulk Flux algorithm 2.0 and transfer coefficients from Fairall et al. (1996b). Meteorological data along with the calculated heat fluxes for the duration of the cruises were used as inputs for the model simulations. Values were interpolated to the resolution of the model time step and input to the model at each time step. The models were initialized with isothermal and constant salinity profiles based on observations from the research vessels at the start time of each run. Model

Near-surface diurnal warming simulationsB. Scanlon et al.

[Title Page](#)[Abstract](#)[Introduction](#)[Conclusions](#)[References](#)[Tables](#)[Figures](#)[◀](#)[▶](#)[◀](#)[▶](#)[Back](#)[Close](#)[Full Screen / Esc](#)[Printer-friendly Version](#)[Interactive Discussion](#)

execution was begun at midnight local solar time the day before the period of the comparison with the observed profiles to allow the model to spin up. While the modeled profiles were allowed to evolve freely, to minimize advective effects, the entire modeled temperature profile was simply shifted at each time step to pass through the measured subsurface temperature from the research vessel at the appropriate depth. The time step employed in the models was one minute. The vertical resolution of the model was 0.02 m between depths 0.03–4.99 m and scaled to 0.15 m for depths thereafter. A finer resolution near the surface defined by temperature values at 0.0025, 0.0075 and 0.015 m depths was used to represent the upper few centimetres of the ocean. To extend temperature estimates from the shallowest layer of the model at 0.0025 m to the skin, the skin layer parameterization of Fairall et al. (1996a) is incorporated in the model.

4 Results

In this section, the model simulations of the five model versions discussed in the previous section are compared to high resolution in-situ measurements. For comparison, the modelled simulated and measured temperature profiles are bin averaged to 2 cm depth intervals, with increased resolution nearer the surface at depths 0, 0.0025, 0.0075, and 0.015 m. The time of day henceforth used in the text is local.

4.1 Model performance in day-time stratification conditions

Observational measurements from GC99 are used in the case of model validation in highly stratified conditions. The average solar irradiance is 802 W m^{-2} (peaking at 912 W m^{-2}) and the mean wind speed is 1.1 m s^{-2} for the duration of the deployment (Fig. 1). Diurnal warming effects are very evident in this dataset with warm-layer depths observed between 0.2–1.0 m throughout this deployment period (Fig. 2, top left). Timeseries plots for the five models show the temporal evolution of the

Near-surface diurnal warming simulations

B. Scanlon et al.

Title Page

Abstract

Introduction

Conclusions

References

Tables

Figures

◀

▶

◀

▶

Back

Close

Full Screen / Esc

Printer-friendly Version

Interactive Discussion



temperature differences between modelled and measured profiles (Fig. 2, column 1). The optimal temperature difference interval ($\pm 0.2\text{K}$) is coloured white in the plots. This interval represents required SST values to compute heat fluxes to within a $\pm 10\text{Wm}^{-2}$ accuracy.

5 The baseline model achieves the highest accuracy of the five models, providing good simulation results for this example of highly stratified conditions. This is mainly due to the baseline model predicting the most accurate warm-layer depth, resulting in a minimal mean temperature difference of 0.05K from $0.5\text{--}5\text{m}$ depth (Fig. 3). All five mixing schemes struggle to resolve the upper half metre correctly. It is important to note that it is difficult to conduct point-to-point comparisons given the potential for advective effects not considered in one dimensional models. It is still interesting, however, to compare the relative performance of the different models. The two blended models achieve the highest temperature differences of the five models with an overestimation of 2.5K for a brief period. This occurs at the beginning of the deployment when the water column was observed to be well mixed (Fig. 2). All the models predict a diurnal warm-layer at 1m depth during this period, which accounts for the simulated temperature overestimations. The blended and baseline models overpredict temperatures during another period between $11:45\text{--}12:15$, when the solar heat flux drops to $\sim 700\text{Wm}^{-2}$ (Fig. 1), presumably due to shading of the incoming shortwave radiation due to a passing cloud (see DSW data in Fig. 1). The observed warm-layer depth deepens by half a metre during this period (Fig. 2, top left). The five models don't simulate this temporary deepening which could be related to their one-dimensional nature. The blended and baseline models strongly overestimate temperature during this period (Fig. 2), which strongly affect the models overall performance. The enhanced models perform well in this brief period, which is due to the overestimated warm-layer depths now matching the observations (Fig. 2).

25 The models are perhaps best compared averaging their performance over multiple events. Mean temperature profiles for the five model versions were computed for the duration of GL99 (Fig. 3). On average the baseline mixing model over-predicts SST_{Skin}

Near-surface diurnal warming simulations

B. Scanlon et al.

Title Page

Abstract

Introduction

Conclusions

References

Tables

Figures

◀

▶

◀

▶

Back

Close

Full Screen / Esc

Printer-friendly Version

Interactive Discussion



value by 0.28 K. The enhanced wave breaking and solar transmission models underpredict SST_{Skin} values by 0.85 K and 1.0 K respectively, for the entire deployment while the blended model overpredicts SST_{Skin} by 0.7 K (Fig. 3). The blended solar transmission model simulates the best results as it underpredicts SST_{Skin} by 0.11 K and also provides the best results down to a depth of ~ 0.1 m.

The enhanced wave breaking and solar transmission models predict larger warm-layer depths than the observed (Fig. 3). This affects the simulations by underestimating temperature within the observed warm-layer and overestimating the temperature approximately 1 m below his layer depth (Fig. 4). This is evident in the EWB and EST plots of Fig. 2, where the yellow coloured areas in the centre of the plots represent the temperature overestimation. This is due to the enhanced models overestimating mixing in the upper few metres. This overestimation of mixing deepens the diurnal thermocline and creates an underestimation in temperature in the layers above which can be observed as the blue coloured areas.

4.2 Model performance in night-time conditions

Observational measurements from GL03 are used to validate model simulations in conditions corresponding to night-time cooling and the initiation of diurnal warming. The deployment started at 23:08 and continued throughout the night until 11:23 the next morning. The mean wind speed is $6.3 \pm 0.5 \text{ m s}^{-1}$ and the solar heat flux steadily rises from 0 to 876 W m^{-2} due to the morning solar heating (Fig. 1).

The plots (Fig. 2, column 2) show the times series of the measured profiles and temperature differences (model minus measured) of the 5 model versions for GL03. Due to the small temperature changes observed, the white temperature difference interval represents 0.1 K for clarity (Fig. 2, column 2). The SkinDeEP data shows a well-mixed water column for most of the deployment period. A warm-layer is formed at $\sim 10:00$ with the increase of morning solar heating. The plot in Fig. 4 shows the mean temperature difference profile of the modelled minus the measured profiles for the deployment.

Near-surface diurnal warming simulations

B. Scanlon et al.

Title Page

Abstract

Introduction

Conclusions

References

Tables

Figures



Back

Close

Full Screen / Esc

Printer-friendly Version

Interactive Discussion



The enhanced models and blended models simulations are almost uniform with depth (Fig. 4).

The five models provide a mean temperature overestimation of 0.05 K from 0.0025–5 m depth, while the baseline model overpredicts by 0.085 K. All the models struggle to simulate the cool skin temperature correctly. The cool skin correction applied in the models was too weak (Fig. 4) and the simulated SST_{Skin} values were overestimated by nearly 0.3 K. It is clear that the enhanced and blended models simulated the depth of the diurnal warm-layer quite well as the temperature difference profile in Fig. 4 is relatively straight. The baseline model simulates a shallow diurnal mixed layer which can be observed in Fig. 4, as the temperature difference curve changes slope rapidly below 2 m depth. Due to this, the temperature has been overestimated near the surface and underestimated below the observed mixed layer (Fig. 2). The enhanced and blended models are within the ± 0.2 K temperature difference. It is evident that the enhanced and blended models produces the best results for this period for night-time well mixed conditions.

4.3 Model performance for day-night transition

ASIP measured temperature profiles from IO07 dataset are used in this study to validate the models performance in the stratified Cirene region of the Indian-Pacific warm pool. The downwelling shortwave radiation and wind speed for this modelling period are illustrated in Fig. 1. The deployment takes place over night-time and continues for a brief period after sunrise. A timeseries plot of the observed temperature structure can be observed (Fig. 2, top right). A diurnal warm-layer exists at 4 m depth at the beginning of the period, slowly deepening until the upper 5 m is well mixed at 02:00. Timeseries plots of the temperature difference for the 5 model versions are shown for this period (Fig. 2, column 3). It is evident that the temperature simulations struggle to replicate observations. The models underestimate the temperature for the first half of the deployment, despite all the models estimating the warm-layer depth accurately

Near-surface diurnal warming simulations

B. Scanlon et al.

Title Page

Abstract

Introduction

Conclusions

References

Tables

Figures

◀

▶

◀

▶

Back

Close

Full Screen / Esc

Printer-friendly Version

Interactive Discussion



at 4 m. Towards the end of the deployment, all models simulate a strong temperature overestimation by as much as 1 K.

The mean temperature profiles for each of the models are shown in Fig. 5. On average all models under-predict the temperature below 1 m. Despite 72 profiles, a high deviation in the mean temperature difference profiles (Fig. 5) occurs for all the models. This is due to the models underestimating temperature during the night and overestimating the temperature after sunrise (Fig. 2). The enhanced wave breaking model produces the best SST_{Skin} estimates with an average difference of 0.1 K from measurements. The blended model also performs well with a average difference of 0.2 K. The enhanced solar transmission, baseline and blended solar transmission models produce less accurate estimates with temperature differences of 0.31 K, 0.38 K and 0.38 K, respectively. The enhanced wave breaking model produces the best results for this deployment with a minimal SST_{Skin} difference for the mean temperature difference evaluation.

The cool skin correction model applied in the simulations produces strongly overestimated SST_{Skin} estimates when compared to the SST_{Skin} directly below the cool skin layer. The correction model produced 0.1 K overestimation for all of the models.

4.4 Overall model performance

In this section, all the available observed profiles (1165) are collectively used to validate the five model versions. A mean temperature profile for these profiles is shown in Fig. 6. A temperature gradient exists at 0.2 m depth, implying that strong effects of stratification are evident. The average diurnal warming from 0.1 to 1 m relative to greatest measured depths is about 0.7 K and slightly less at the ocean skin.

The mean temperature difference profiles for the five models using all of the available profiles which are discussed in Sect. 2.1 are shown in Fig. 7. The conditions are mixed in a low to moderate wind environment and with strong solar heating present (Fig. 1). The majority of deployments show strong characteristics of stratification in the water column (Fig. 6). Overall, the baseline model simulations provide the most accurate

Near-surface diurnal warming simulations

B. Scanlon et al.

Title Page

Abstract

Introduction

Conclusions

References

Tables

Figures

◀

▶

◀

▶

Back

Close

Full Screen / Esc

Printer-friendly Version

Interactive Discussion



Near-surface diurnal warming simulations

B. Scanlon et al.

[Title Page](#)[Abstract](#)[Introduction](#)[Conclusions](#)[References](#)[Tables](#)[Figures](#)[◀](#)[▶](#)[◀](#)[▶](#)[Back](#)[Close](#)[Full Screen / Esc](#)[Printer-friendly Version](#)[Interactive Discussion](#)

SST_{Skin} values with a slight mean overestimation of 0.024 K. The blended model also works well with a mean overestimation of 0.07 K. The enhanced models show strong temperature underestimations throughout the warm-layer (Fig. 7) which strongly affects the cool-skin temperature estimations. The enhanced models underestimate SST_{Skin} by 0.27 K. The blended solar transmission model underestimates SST_{Skin} by 0.08 K.

Comparing Figs. 6 and 7, it is clear that the baseline model predicts the most accurate mixed-layer depth, within negligible temperature variations up to 0.1 m depth. A minor temperature overestimation occurs above 0.1 m depth for the baseline and blended model versions, caused by the use of the 9-band solar absorption model. The addition of the OS00 solar transmission model corrects this warming overestimation above this depth, which can be observed from the temperature profile simulated by the blended solar transmission model in Fig. 7.

The blended solar transmission model performs the best for depths from the subskin to ~0.1 m. The enhanced models show strong temperature underestimations above 0.2 m depth, influenced by the increased mixing parameters associated with the addition of the KC04 enhancement. The little difference between the results from the two enhanced model versions implies that the OS00 solar transmission enhancement has a low impact on the results compared to that of the KC04 enhancement.

The cool-skin correction in the plot (Fig. 7) is very strong for all the models. It causes an underestimation of 0.09 K with respect to the warm-layer correction. In particular, this has a strong impact on the overall performance of the blended solar transmission model.

5 Conclusions

A strong variability in the results was shown to exist between the models for highly stratified conditions (Fig. 3). Overall, the baseline model produces the most accurate temperature estimates for the cruise periods used in this study. The enhanced models showed a strong temperature underestimation in the diurnal mixed layer for simulations

Near-surface diurnal warming simulations

B. Scanlon et al.

Title Page

Abstract

Introduction

Conclusions

References

Tables

Figures

◀

▶

◀

▶

Back

Close

Full Screen / Esc

Printer-friendly Version

Interactive Discussion



- Donlon, C. J.: Radiometric Observations of the Sea Surface and Atmosphere (ROSSA) Cruise, Report and Data Summary, Joint Res. Centre, Brussels, Belgium, 1999. 3854
- Donlon, C. J., Minnett, P. J., Gentemann, C., Nightingale, T. J., Barton, I. J., Ward, B., and Murray, J.: Toward improved validation of satellite sea surface skin temperature measurements for climate research, *J. Climate*, 15, 353–369, 2002. 3853
- Fairall, C. W., Bradley, E. F., Godfrey, J. S., Wick, G. A., Edson, J. B., and Young, G. S.: Cool-skin and warm-layer effects on sea surface temperature, *J. Geophys. Res.*, 101, 1295–1308, 1996a. 3852, 3854, 3860
- Fairall, C. W., Bradley, E. F., Rogers, D. P., Edson, J. B., and Young, G. S.: Bulk Parameterization of air–sea fluxes for Tropical Ocean–Global Atmosphere, Coupled–Ocean Atmosphere Response Experiment, *J. Geophys. Res.*, 101, 3747–3764, 1996b. 3852, 3853, 3859
- Gentemann, C. L. and Minnett, P. J.: Radiometric measurements of ocean surface thermal variability, *J. Geophys. Res.*, 113, C08017, doi:10.1029/2007JC004540, 2009. 3854
- Gentemann, C. L., Minnett, P. J., and Ward, B.: Profiles of ocean surface heating (POSH): A new model of upper ocean diurnal warming, *J. Geophys. Res.*, 114, C07017, doi:10.1029/2008JC004825, 2009. 3853, 3854
- Kantha, L. H.: On an improved model for the turbulent PBL, *J. Atmos. Sci.*, 60, 2239–2246, 2003. 3858
- Kantha, L. H. and Clayson, C. A.: An improved mixed layer model for geophysical applications, *J. Geophys. Res.*, 99, 25235–25266, 1994. 3854, 3857
- Kantha, L. H. and Clayson, C. A.: On the effect of surface gravity waves on mixing in the oceanic mixed layer. *Ocean Modelling, Ocean Modell.*, 6, 101–124, 2004. 3854, 3858, 3866
- Minnett, P. J., Knuteson, R. O., Best, F. A., Osborne, B. J., Hanafin, J. A., and Brown, O. B.: The Marine-Atmospheric Emitted Radiance Interferometer (M-AERI), a high accuracy, seagoing infrared spectroradiometer., *J. Atmos. Ocean. Technol.*, 18, 994–1013, 2001. 3857
- Ohlmann, J. C. and Siegel, D. A.: Ocean Radiant heating. Part II: Parameterizing solar radiation transmission through the upper ocean, *J. Phys. Oceanogr.*, 30, 1849–1865, 2000. 3854, 3859, 3866
- Ohlmann, J. C., Siegel, D. A., and Washburn, L.: Radiant heating of the western equatorial Pacific during TOGA-COARE, *J. Geophys. Res.*, 103, 5379–5395, 1998. 3858
- Paulson, C. A. and Simpson, J. J.: The temperature difference across the coolskin of the ocean, *J. Geophys. Res.*, 86, 11044–11054, 1981. 3857, 3858

Near-surface diurnal warming simulations

B. Scanlon et al.

Title Page

Abstract

Introduction

Conclusions

References

Tables

Figures

◀

▶

◀

▶

Back

Close

Full Screen / Esc

Printer-friendly Version

Interactive Discussion



- Price, J. F., Weller, R. A., and Pinkel, R.: Diurnal cycling: Observations and models of the upper ocean response to diurnal heating, cooling and wind mixing, *J. Geophys. Res.*, 91, 8411–8427, 1986. 3853
- 5 Soloviev, A. and Schluessel, P.: Evolution of cool skin and direct air-sea gas transfer coefficient during daytime, *Bound.-Lay. Meteorol.*, 77, 45–68, 1996. 3854
- Soloviev, A. V. and Lukas, R.: Observation of spatial variability of diurnal thermocline and rain-formed halocline in the western Pacific warm pool, *J. Phys. Oceanogr.*, 26, 2529–2538, 1996. 3853
- 10 Stramma, L., Cornillon, P., Weller, R. A., Price, J. F., and Briscoe, M.: Large diurnal sea surface temperature variability: satellite and in situ measurements, *J. Phys. Oceanogr.*, 16, 827–837, 1986. 3853
- Terray, E. A., Donelan, M. A., Agrawal, Y. C., Drennan, W. M., Kahma, K. K., A. J. Williams III, Hwang, P. A., and Kitaigorodskii, S. A.: Estimates of kinetic energy dissipation under breaking waves, *J. Phys. Oceanogr.*, 26, 792–807, 1996. 3858
- 15 Vialard, J., Duvel, J.-P., McPhaden, M., Bouruet-Aubertot, P., Ward, B., Key, E., Bourras, D., Weller, R., Minnett, P., Weill, A., Cassou, C., Eymard, L., Fristedt, T., Basdevant, C., Dandoneau, Y., Duteil, O., Izumo, T., de Boyer Montégut, C., and Masson, S.: Cirene: Air-sea interactions in the Seychelles-Chagos thermocline ridge region, *Bull. Amer. Meteorol. Soc.*, 90, 45–61, doi:10.1175/2008BAMS2499.1, 2009. 3855
- 20 Ward, B.: Near-surface ocean temperature, *J. Geophys. Res.*, 109, C02004, doi:10.1029/2004JC002689, 2006. 3855, 3856
- Ward, B., Wanninkhof, R., McGillis, W. R., Jessup, A. T., DeGrandpre, M. D., Hare, J. E., and Edson, J. B.: Biases in the air-sea flux of CO₂ resulting from ocean surface temperature gradients, *J. Geophys. Res.*, 109, C08S08, doi:10.1029/2003JC001800, 2004a. 3852
- 25 Ward, B., Wanninkhof, R., Minnett, P. J., and Head, M.: SkinDeEP: A Profiling Instrument for Upper Decameter Sea Surface Measurements, *J. Atmos. Ocean. Technol.*, 21, 207–222, 2004b. 3854, 3856
- Ward, B., Fristedt, T., Callaghan, A. H., Sutherland, G., Sanchez, X., Vialard, J., and Lilley, J. M.: The Air-Sea Interaction Profiler (ASIP): An Autonomous Upwardly-Rising Profiler for Microstructure Measurements in the Upper Ocean, *J. Atmos. Ocean. Technol.*, in preparation, 2012. 3854, 3856
- 30 Webster, P. J., Clayson, C. A., and Curry, J. A.: Clouds, radiation, and the diurnal cycle of sea surface temperature in the tropical western Pacific, *J. Climatol.*, 9(8), 1712–1730, 1996. 3854

Weller, R. and Price, J. F.: Langmuir circulations in the oceanic surface layer, *Deep-Sea Res.*, 35, 711–747, 1988. 3858

5 Wick, G. A., Emery, W. J., Kantha, L. H., and Schlüssel, P.: The behavior of the bulk–skin sea surface temperature difference under varying wind speed and heat flux, *J. Phys. Oceanogr.*, 26, 1969–1988, 1996. 3853

Near-surface diurnal warming simulations

B. Scanlon et al.

Title Page

Abstract

Introduction

Conclusions

References

Tables

Figures

⏪

⏩

◀

▶

Back

Close

Full Screen / Esc

Printer-friendly Version

Interactive Discussion



Near-surface diurnal warming simulations

B. Scanlon et al.

Title Page

Abstract

Introduction

Conclusions

References

Tables

Figures

◀

▶

◀

▶

Back

Close

Full Screen / Esc

Printer-friendly Version

Interactive Discussion



Table 1. Times, location and number of profiles for the deployments of the three case studies.

Region	Date	Time (Local)	Latitude	Longitude	# of profiles
GC99	283	11:12–14:13	22°31.48 N	109°35.43 W	161
GL03	113/114	23:08–11:23	42°18.47 N	5°05.65 E	117
IO07	39/40	19:02–7:20	7°59.77 S	67°27.70 E	72

Near-surface diurnal warming simulations

B. Scanlon et al.

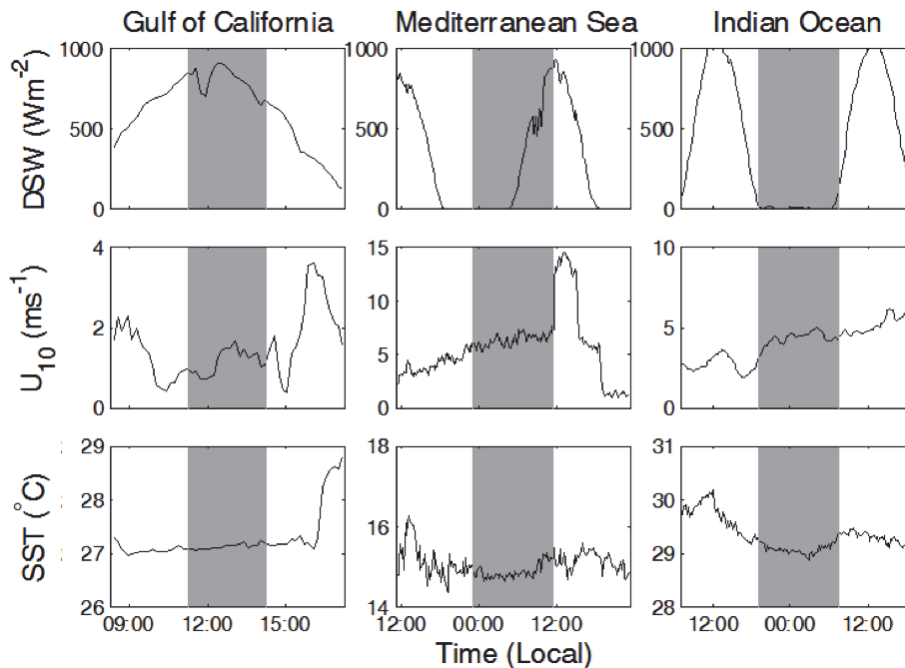


Fig. 1. Time series of the downwelling shortwave radiation, wind speed, and skin temperature for the GC99, GL03 and IO07 periods respectively. The grey vertical column marks the time of the deployment period. The data is 60 min averaged.

[Title Page](#)
[Abstract](#)
[Introduction](#)
[Conclusions](#)
[References](#)
[Tables](#)
[Figures](#)
[◀](#)
[▶](#)
[◀](#)
[▶](#)
[Back](#)
[Close](#)
[Full Screen / Esc](#)
[Printer-friendly Version](#)
[Interactive Discussion](#)


Near-surface diurnal warming simulations

B. Scanlon et al.

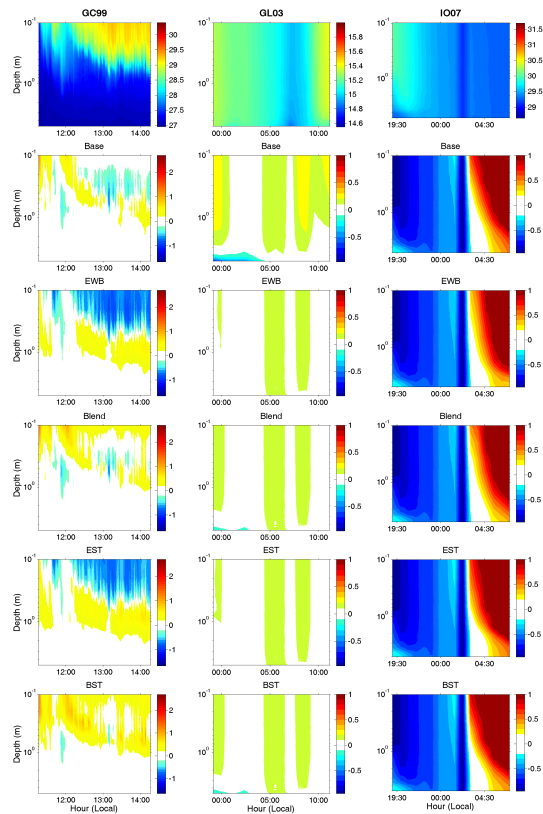


Fig. 2. Columned timeseries plots for the respective case studies. The first row shows the observed temperature plots. The remaining rows show the temperature difference (modelled minus observed) plots for the 5 model versions. The white area used represents an ideal ΔT of $\pm 0.2\text{K}$ for both GC99 and IO07, and a ΔT of $\pm 0.1\text{K}$ for GL03.

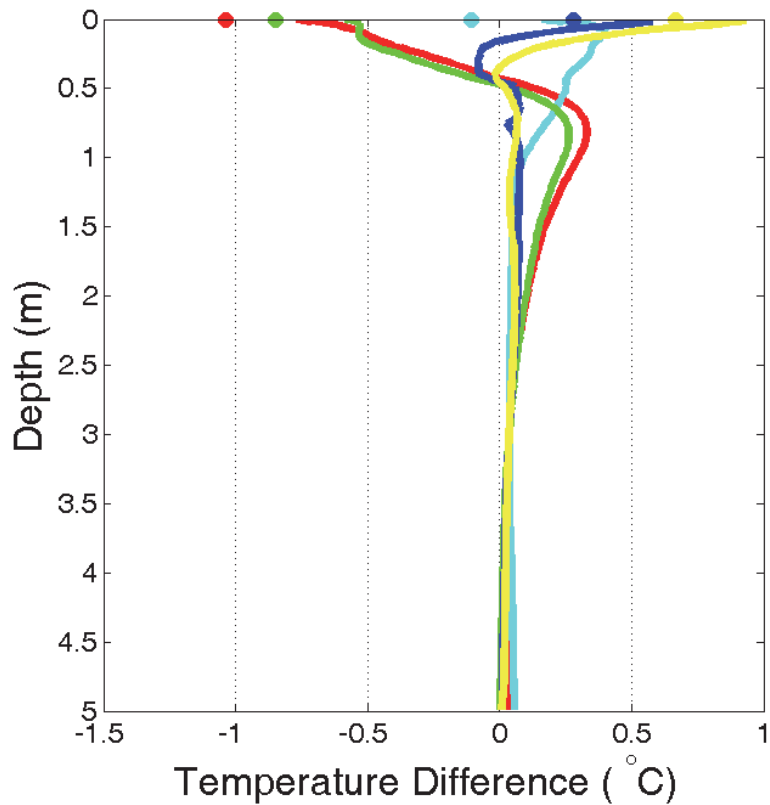


Fig. 3. Mean modelled minus measured temperature difference profiles for the GC99 dataset. The blue, yellow, green, red and cyan profiles represent the mean temperature difference profiles of the base, blend, EWB, EST and BST models, respectively.

Near-surface diurnal warming simulations

B. Scanlon et al.

Title Page	
Abstract	Introduction
Conclusions	References
Tables	Figures
◀	▶
◀	▶
Back	Close
Full Screen / Esc	
Printer-friendly Version	
Interactive Discussion	



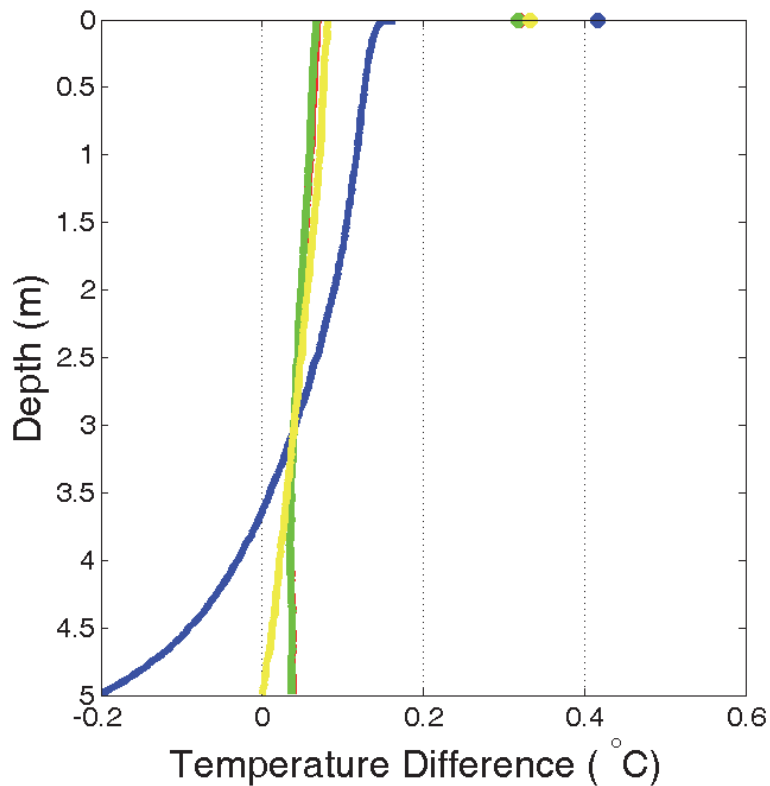


Fig. 4. Mean temperature difference profile for the GL03 dataset. The blue, yellow, green, red and cyan profiles represent the mean temperature difference profiles of the base, blend, EWB, EST and BST models, respectively.

Near-surface diurnal warming simulations

B. Scanlon et al.

Title Page

Abstract Introduction

Conclusions References

Tables Figures

◀ ▶

◀ ▶

Back Close

Full Screen / Esc

Printer-friendly Version

Interactive Discussion



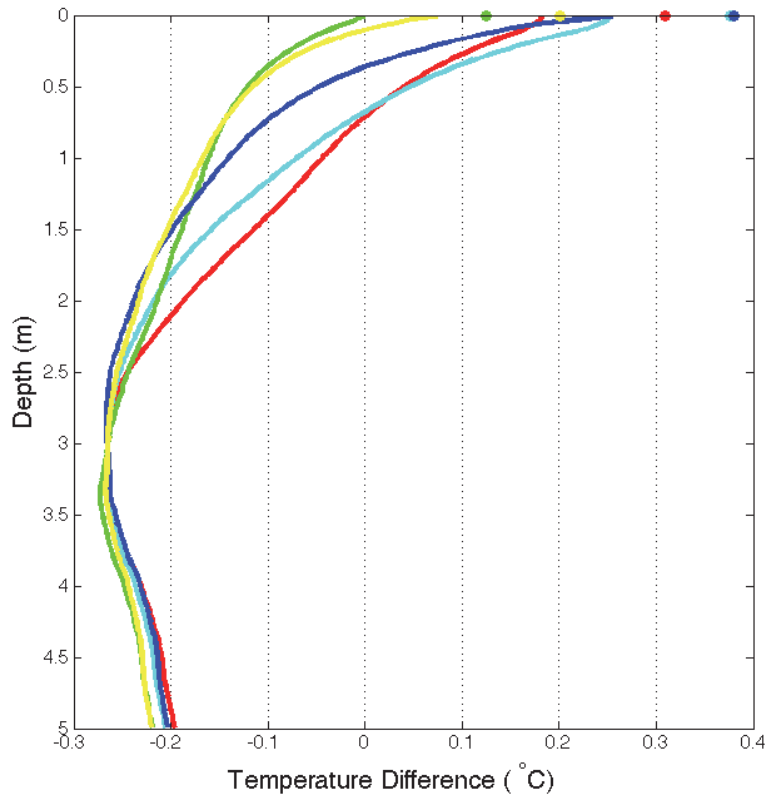


Fig. 5. Mean temperature difference profile for the IO07 dataset. The blue, yellow, green, red and cyan profiles represent the mean temperature difference profiles of the base, blend, EWB, EST and BST models, respectively.

Near-surface diurnal warming simulations

B. Scanlon et al.

Title Page	
Abstract	Introduction
Conclusions	References
Tables	Figures
◀	▶
◀	▶
Back	Close
Full Screen / Esc	
Printer-friendly Version	
Interactive Discussion	



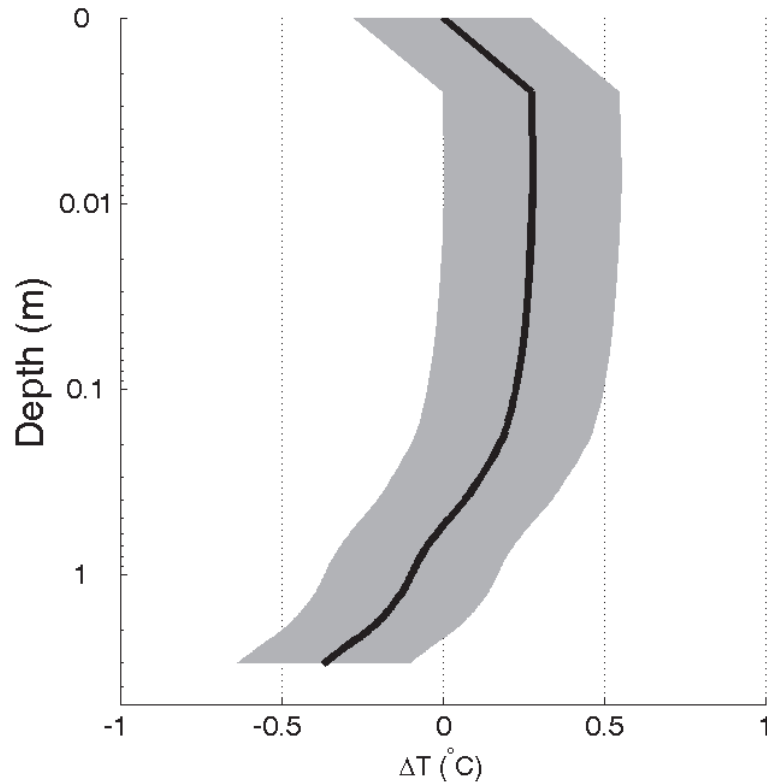


Fig. 6. Mean observed temperature profile for all available data (1165 profiles collectively from GC99, GL03 and IO07 datasets). Mean temperature is normalised to the mean SST_{Skin} value. The shaded region represents the 95 % confidence interval.

Near-surface diurnal warming simulations

B. Scanlon et al.

Title Page	
Abstract	Introduction
Conclusions	References
Tables	Figures
◀	▶
◀	▶
Back	Close
Full Screen / Esc	
Printer-friendly Version	
Interactive Discussion	



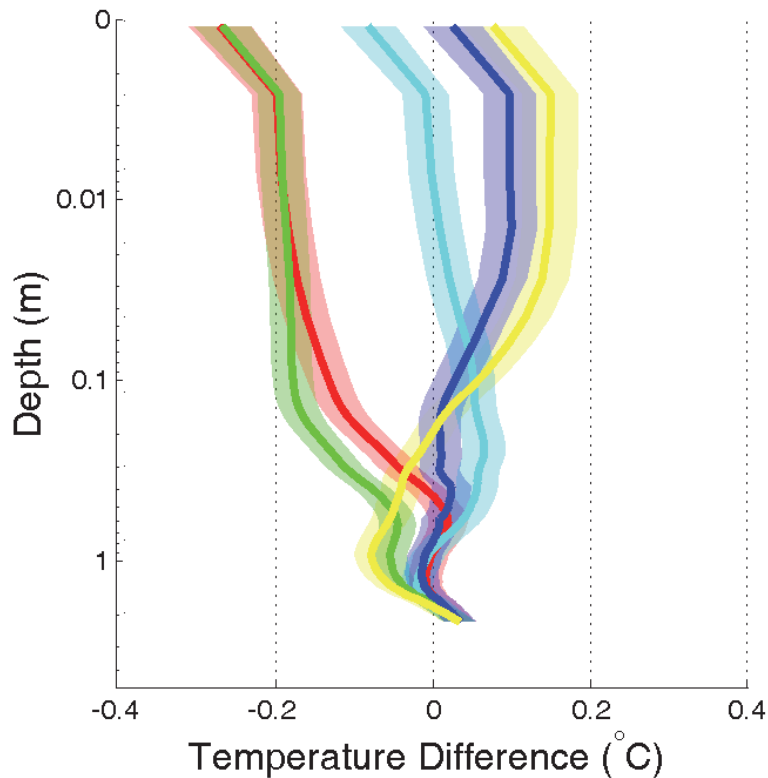


Fig. 7. Mean temperature difference profile for all available data (1165 profiles collectively from the GC99, GL03 and IO07 datasets). The blue, yellow, green, red and cyan profiles represent the mean temperature difference profiles of the base, blend, EWB, EST and BST models, respectively. The transparent colour-coded regions represent the 95 % confidence intervals.

Near-surface diurnal warming simulations

B. Scanlon et al.

Title Page	
Abstract	Introduction
Conclusions	References
Tables	Figures
◀	▶
◀	▶
Back	Close
Full Screen / Esc	
Printer-friendly Version	
Interactive Discussion	

